Food Chemistry 382 (2022) 132349

Contents lists available at ScienceDirect

Food Chemistry

journal homepage: www.elsevier.com/locate/foodchem

Investigation on detoxication effects of 2-hydroxypropyl-β-cyclodextrin over two halogenated aromatic DBPs 2,4,6-trichlorophenol and 2,4,6-tribromophenol binding with human serum albumin

Zhenxuan Zhang [a,b], Qingyao Zhu [a], Wenjie Liang [a], Zekun Han [a], Cui Huang [a], An Liu [a], Yujuan Lu [a], Jiang Ma [b], Mengting Yang [a,*]

[a] College of Chemistry and Environmental Engineering, Shenzhen University, Shenzhen 518060, China
[b] College of Mechatronics and Control Engineering, Shenzhen University, Shenzhen 518060, China

ARTICLE INFO

Keywords:
Disinfection byproducts
Halophenols
Binding interaction
Detoxication
HSA

ABSTRACT

The health effects of disinfection byproducts (DBPs) in drinking water drew great attention recently. Herein, by using *in vitro* (fluorescence quenching, UV absorbance, circular dichroism) and *in silico* (molecular docking) method, binding interactions of two halophenolic DBPs (2,4,6-trichlorophenol [TCP] and 2,4,6-tribromophenol [TBP]) with human serum albumin (HSA) and the influence of hydroxypropyl-beta-cyclodextrin (HPCD) on the interactions were investigated. TCP/TBP could form complexes with HSA mainly by hydrogen bonding, while changing its secondary structure, among which TBP showed more influential effect. Interestingly, the binding constants for halophenol-HSA complexes decreased obviously with the involvement of HPCD. Molecular docking results revealed that HPCD could include TCP/TBP into its cavity and change their original binding sites from subdomain IB to IIA, resulting in a more stable binding system. These findings are beneficial for understanding the toxicity of halophenols inside the human body and indicated that HPCD could be a promising detoxication agent for DBPs.

1. Introduction

Drinking clean water is important for the health of human beings. As the greatest public health triumph, drinking water disinfection plays a significant role in reducing the occurrence and death of infectious diseases caused by pathogenic microorganisms (Richardson, 2003). However, when disinfectant (e.g., chlorine) reacts with natural organic matter and/or bromide ion/iodide ion in water, disinfection byproducts (DBPs) will be generated in drinking water, which pose potential harm to human health (Chu, Li, Gao, Templeton, Tan, & Gao, 2015). Actually, DBPs could also be considered as one important series of food contaminants which will be unavoidably intake by human beings in daily life through direct drinking, washed vegetables/fruits and coffee/tea/juices prepared with tap water (Li, Wang, Chen, Hu, Gong, & Xian, 2019). Epidemiological studies have illustrated that DBP exposure potentially raises health risks, e.g., colorectal/bladder cancer and adverse birth outcomes (Grellier, Rushton, Briggs, & Nieuwenhuijsen, 2015). Hence, increasing concerns have been paid for DBPs owing to their adverse health effects in recent years, especially for some new DBPs, e.g., halogenated aromatic DBPs (Zhang, et al., 2020). Though their occurrence in drinking water may be lower than regulated aliphatic DBPs but certain levels of higher toxicity could be found for these DBPs (Liu, Zhang, Li, Li, Hang, & Sharma, 2019; Zhang, et al., 2020).

No matter for regulated aliphatic DBPs or new aromatic DBPs, many studies have been reported over their toxicity by using different kinds of *in vitro* and *in vivo* bioassays. Yang and Zhang investigated the comparative toxicity of new aromatic DBPs and regulated DBPs by using *in vivo* toxicity bioassays with marine polychaete and the results indicated that the new aromatic DBPs showed significantly (tens to hundreds) higher toxicity level than aliphatic DBPs (Yang & Zhang, 2013). The same conclusions could also be found for toxicity evaluation by *in vivo* method using autotrophic algae *Tetraselmis marina* (Liu, Zhang, Li, Li, Hang, & Sharma, 2019). Our previous work selected human serum albumin (HSA) as a model protein and investigated its interactions with two bromo-phenolic aromatic DBPs, 4-bromophenol or 2,4-dibromophenol, which successfully proved to be an *in vitro* method that can be used to indicate toxicity level (Zhang et al., 2019). Several studies also support our conclusions that investigation of HSA-ligand binding

* Corresponding author.
E-mail address: yangmt@szu.edu.cn (M. Yang).

https://doi.org/10.1016/j.foodchem.2022.132349
Received 22 May 2021; Received in revised form 30 January 2022; Accepted 1 February 2022
Available online 5 February 2022

interactions is crucial in understanding of transport, biological activity, delivery, and clearance of a toxic substance from human body (Sun, Yang, Tang, Liu, Wang, & Li, 2018; Zhang, Guan, Zhang, Yang, Wang, & Peng, 2021; Zhang et al., 2018). However, little information could be found from literature focused on toxicity reduction of DBPs in terms of food additives added to water-related food stuff. Considering them as important series of food contaminants, it would be great for us to find a non-toxic food additive that can lower down the toxicity level of DBPs, as well as to decrease the health risks of DBPs over the human being. Based on the literature study, cyclodextrins (CDs) could potentially be this ideal candidate.

CDs are a group of water-soluble cyclic oligomers, consisting of various D-glucose units with the most commonly used CDs called as α-, β-, and γ-CD, respectively (Davis & Brewster, 2004). With their unique structure of a hydrophobic interior and a hydrophilic rim, CDs have been widely used for pharmacy, catalysis, biotechnology, agriculture, textiles, and the environment owing to the ability to include guest molecules into their cavity to modify their physical and biological properties with non-toxic characteristic and good biocompatibility (Crini, 2014). Thus, it is speculated that CDs may be able to decrease the toxicity level of DBPs. To testify this hypothesis, the *in vitro* bioassay model by using HSA as a target protein to comparatively evaluate the toxicity of different DBPs (Zhang, et al., 2019) was applied in the present study. 2,4,6-trichlorophenol (TCP) and 2,4,6-tribromophenol (TBP) were selected as model DBP compounds considering that both of them could be frequently detected in drinking waters and showed generally higher toxic potencies among different kinds of aromatic DBPs (Yang & Zhang, 2013; Zhang, et al., 2020). Thus, the influence of CDs over the binding behaviors between DBPs and HSA are the major concerns in this study. One typical representative of CDs, 2-hydroxypropyl-β-cyclodextrin (HPCD), which is non-toxic and has relatively higher water solubility (Zhang, Liu, Yang, Chen, & Jiao, 2017), was selected as model CD compound.

Accordingly, the objectives of the present study were to investigate (1) the binding behaviors between TCP/TBP and HSA under simulated physiological conditions of human blood, and (2) the influence of HPCD on the binding behaviors between TCP/TBP and HSA, by using *in vitro* method (fluorescence spectrometry, UV–visible absorption spectrometry, circular dichroism spectroscopy) and *in silico* method (molecular docking). The results of the present study would provide valuable suggestions for possible toxicity reduction of DBPs by using HPCD.

2. Materials and methods

2.1. Chemicals and regents

HSA (≥96%) and HPCD (≥98%) were acquired from J & K chemical (China), whereas TCP (99%) and TBP (98%) were obtained from Sigma-Aldrich (USA). Tris-HCl buffer of pH = 7.4 was procured from Solarbio (China). *p*-nitrophenyl acetate (98%) was purchased from Macklin (China). They were analytical grade and used as received without further purification. Ultrapure water was used throughout the experiments.

2.2. Sample preparation

The stock solution of HSA (1.0 mmol/L) was prepared by tris-HCl buffer of pH = 7.4, and TCP/TBP stock solution (1.0 mmol/L) was prepared in ethanol. The concentration of HSA was analyzed by using UV–vis absorbance spectroscopy (Rabbani et al., 2017). All stock solutions were stored in the refrigerator at 4 °C and working solutions were serial diluted from stock solutions before use. The *in vitro* analysis were carried out in simulative physiological condition with a fixed amount of 0.9% (w/v) NaCl concentration and 1 μmol/L HSA, while constantly changing TCP/TBP concentrations in different conditions.

2.3. Fluorescence spectroscopy analysis

Lumina fluorescence spectrophotometer (Thermo, Germany) equipped with a 150 W Xenon lamp and a circulating water bath to maintain required temperatures was used to perform spectroscopy measurements. Slit widths of 5.0 nm and 5.0 nm were set for the excitation and emission measurement by using a 1-cm quartz cell. The scan speed was set at 600 nm/min and photo multiplier tube voltage set as 700 V, respectively. The excitation wavelength of HSA was set at 280 nm at temperatures of 296, 303, 310, and 318 K and emission spectra were recorded in the range of 300–500 nm. Fluorescence lifetime of HSA was measured by using an Edinburg FLS-1000 spectrofluorimeter at temperatures of 296 K.

2.4. Isothermal titration calorimetry (ITC) analysis

ITC was measured with a MicroCal iTC200 titration microcalorimeter (Malvern Panalytical, USA) in order to calculate the thermodynamics parameters for halophenol-HSA interactions as comparison to fluorescence quenching. The thermodynamics parameters were analyzed at a temperature of 37 ℃ by conducting 19 injections of 2 μL TCP/TBP solutions. The ITC cell's stirring speed was set as 750 rpm, and reference power 5 μcal/s.

2.5. Esterase-like activity assay

The influence of TCP/TBP on the esterase-like activity of HSA (5 μmol/L) with and without the presence of HPCD (0.5 mmol/L) was investigated by reaction with varying concentrations (0.1–0.8 mmol/L) of *p*-nitrophenyl acetate (*p*-NPA) at 310 K. The concentrations of HSA: (TCP/TBP) were set with ratios of 1:0, 1:5, 1:10, respectively. After reacting for 2 h, the absorbance of the released product *p*-nitrophenol was measured at 405 nm by using Evolution 220 UV–vis spectrophotometer (Thermo, Germany) with a slit width of 1.0 nm. The initial reaction velocities (v_0) were calculated from the slope of the absorbance in the first two minutes reaction period. The kinetic parameters (K_m, v_{max} and k_{cat}) were calculated by using Michaelis-Menten equation according to the literature (Rabbani, Baig, Lee, Cho, Ma, & Choi, 2017).

2.6. UV–visible absorption analysis

The UV absorbance spectra of HSA in different conditions were recorded from 200 to 400 nm at the temperature of 296 K in a 1-cm quartz cell with a slit width of 1.0 nm by using Evolution 220 UV–vis spectrophotometer (Thermo, Germany).

2.7. Circular dichroism analysis

The circular dichroism spectra were acquired from 200 to 260 nm at the temperature of 296 K with a 1-mm quartz cell by using Chirascan spectropolarimeter (Applied Photophysics, UK). Three successive scans were performed to obtain each circular dichroism spectrum.

2.8. Molecular docking analysis

Molecular docking by using Autodock 4.2 (Morris et al., 2009) was adopted to study the binding interactions between TCP/TBP and HSA (PDB code: 1H9Z) (Petitpas, Bhattacharya, Twine, East, & Curry, 2001) at molecular level. TCP and TBP optimized structures were acquired from Gaussian 09 by using density functional theory (DFT) method at the B3LYP/6–311 + G (d,p) level (Frisch, et al., 2009). Gasteiger charges and polar hydrogens were added to the HSA macromolecule prior to docking. The crystal HPCD structure was constructed by adding hydroxy-propyl chains and hydrogen atoms to the β-CD (PDB code: 2Y4S) structure (Vester-Christensen, Hachem, Svensson, & Henriksen, 2010). Blind docking was performed by using a grid box with spacing

1.000 Å and size of 100 Å, 100 Å, 100 Å along x, y and z axes, respectively. The Lamarckian genetic algorithm (LGA) method with good efficiency and reliability was chosen to perform ligand conformational searching and implement molecular docking (Morris et al., 1998). The docking parameters were set as follows: docking trials, 100; population size, 150; energy evaluations, 2500000. Pymol 1.7 was adopted to visualize and analyze the optimized binding mode with the lowest binding affinity among all the possible binding modes generated for each of halophenol-HSA, halophenol-HPCD or halophenol-HPCD-HSA complexes.

3. Results and discussion

3.1. Fluorescence quenching

The fluorescence quenching method has been proved to be an effective method to investigate the protein–ligand interactions and the structure information of relative protein (Rabbani, Ahmad, Khan, Ashraf, Bhat, & Khan, 2015). Generally, the intrinsic fluorescence of HSA is contributed by 3 residues, i.e., tryptophan (Trp), tyrosine (Tyr) and phenylalanine, but actually dominated by only Trp residue (Rabbani & Ahn, 2019). The quenching of intrinsic fluorescence of protein by ligands indicated the binding of ligand to the protein. Fig. 1a–h shows the effects of increasing concentration of TCP/TBP on the intrinsic HSA fluorescence intensity at temperatures of 296, 303, 310, and 318 K. For either TCP or TBP, as a ligand (TCP/TBP) concentration increased, the emission fluorescence maxima of HSA at λ = 346 nm decreased regularly, implying that TCP/TBP could quench the intrinsic fluorescence of HSA macromolecule through binding interactions. Interestingly, after addition of HPCD to the TCP/TBP-HSA binding system, it can be clearly seen from the graph that the degree of quenching effect for HSA largely decreased (Fig. 2a–h), indicating that HPCD could hinder the interactions between TCP/TBP and HSA.

3.2. Quenching mechanism and binding parameters

The fluorescence quenching mechanisms could be well described by two different patterns, static quenching (complex formation) and dynamic quenching (molecular collision) which are temperature dependent (Rabbani, Baig, Lee, Cho, Ma, & Choi, 2017). With the temperature of binding system increases, the fluorescence quenching constant gradually decreases for static quenching, and the opposite phenomenon for dynamic quenching (Rabbani, Khan, Ahmad, Maskat, & Khan, 2014). To further understand the mechanism of fluorescence quenching effect of the TCP/TBP-HSA system, fluorescence quenching constants were calculated as follows. Correction of the inner filter effect for fluorescence signal was carried out by using the following equation (Ye, et al., 2020):

$$CF = \frac{F_{cor}}{F_{obs}} = \frac{2.3dA_{ex}}{1-10^{-dA_{ex}}} \times 10^{gA_{em}} \times \frac{2.3sA_{em}}{1-10^{-sA_{em}}} \quad (1)$$

where CF stands for the corrected factor, F_{cor} and F_{obs} represent the corrected and measured fluorescence intensity, the details for inner filter effect correction can be found in Supplementary Materials (Fig. S1). The classical Stern-Volmer equation was adopted for fitting analysis of the fluorescence data after inner filter effect correction (Eftink & Ghiron, 1981):

$$\frac{F_0}{F} = 1 + k_q\tau_0[Q] = 1 + K_{sv}[Q] \quad (2)$$

where F and F_0 are the fluorescence intensities of HSA with and

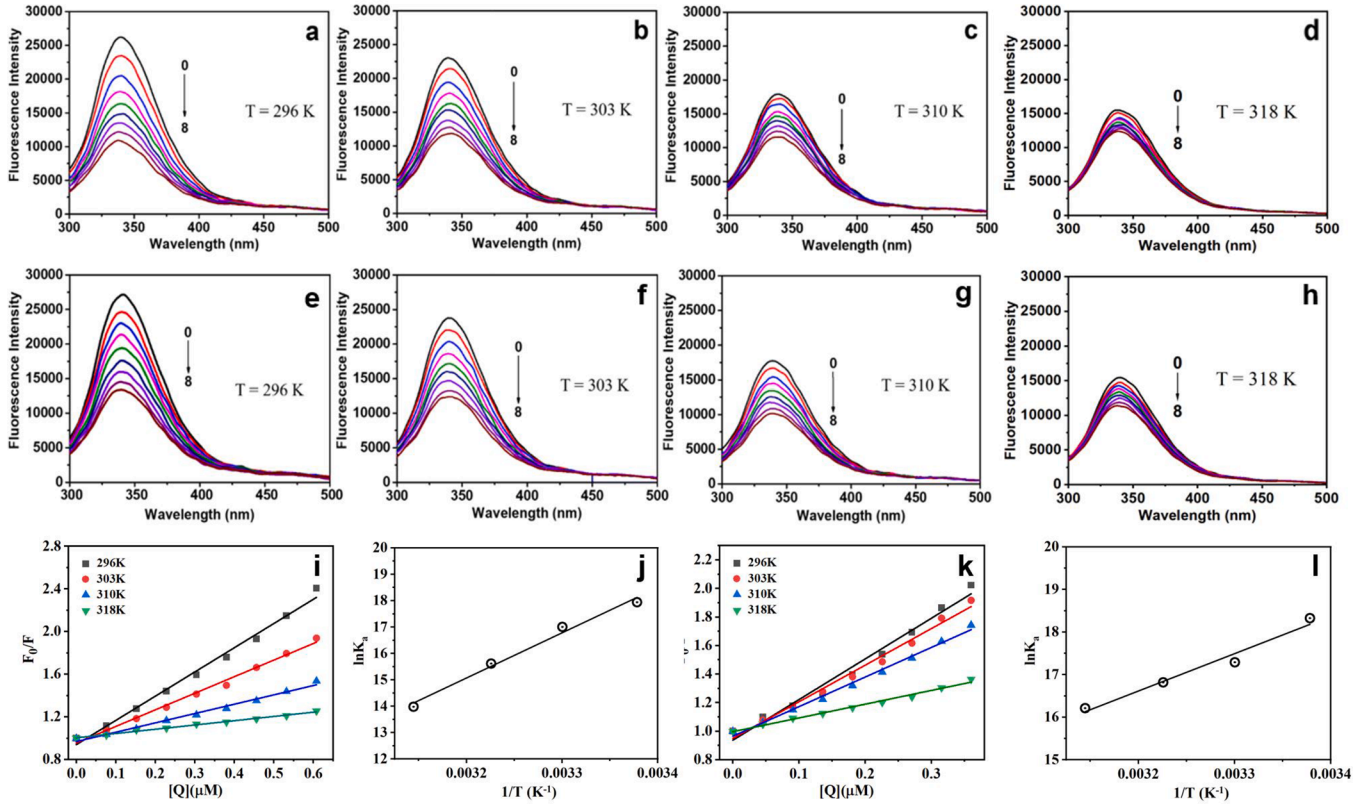

Fig. 1. (a–d) Fluorescence emission spectra of HSA (1 μmol/L) in the absence and presence of increasing concentrations of TCP (0–8: 0–120 μg/L with 15 μg/L intervals) at 296, 303, 310 and 318 K, respectively. (e–h) Fluorescence spectra of HSA (1 μmol/L) in the absence and presence of increasing concentrations of TBP (0–8: 0–120 μg/L with 15 μg/L intervals) at 296, 303, 310 and 318 K, respectively. (i) Stern-Volmer plots for the TCP-HSA interaction at 296, 303, 310 and 318 K, respectively. (j) Van't Hoff plot for the TCP-HSA interaction. (k) Stern-Volmer plots for the TBP-HSA interaction at 296, 303, 310 and 318 K, respectively. (l) Van't Hoff plot for the TBP-HSA interaction.

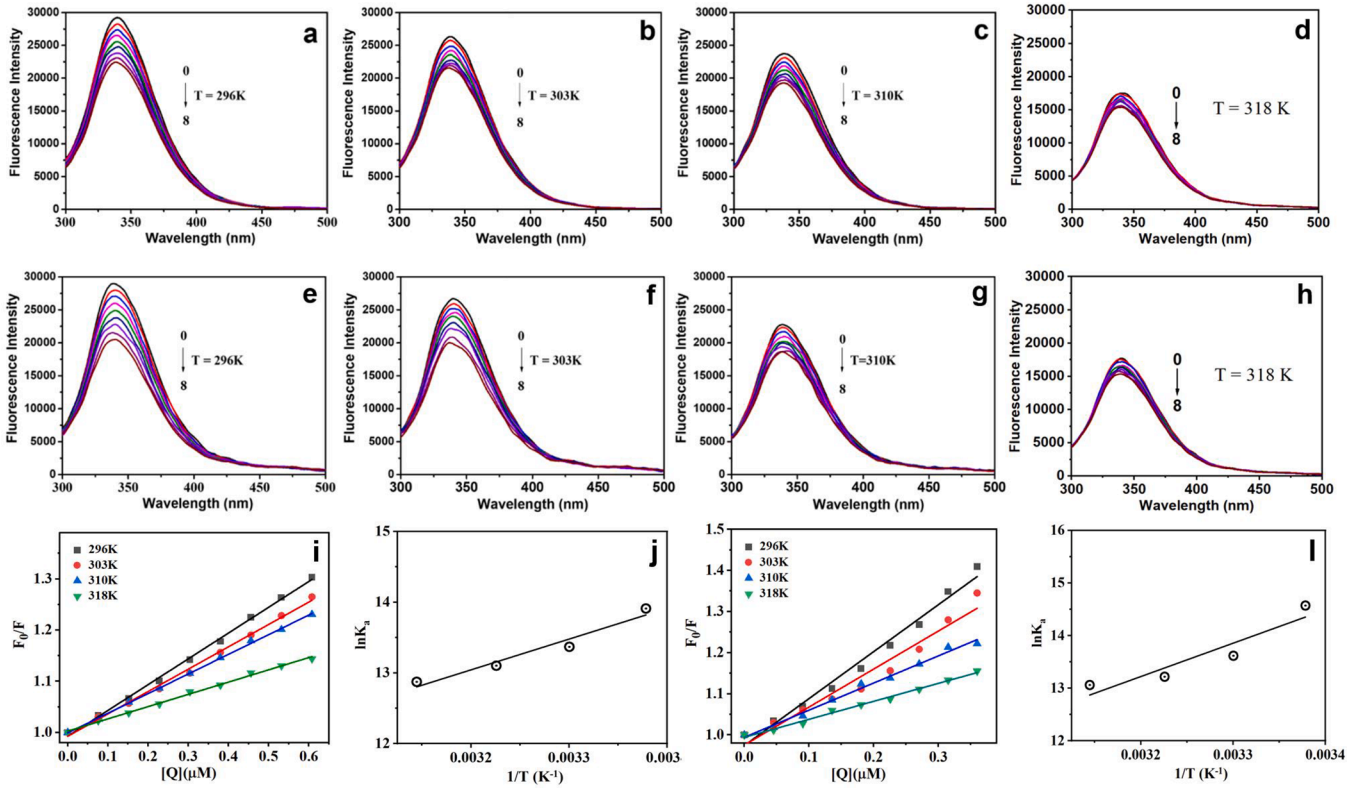

Fig. 2. (a–d) Fluorescence emission spectra of HSA (1 μmol/L) in the absence and presence of increasing concentrations of TCP (0–8: 0–120 μg/L with 15 μg/L intervals) after addition of HPCD (0.5 mmol/L) at 296, 303, 310 and 318 K, respectively. (e−h) Fluorescence spectra of HSA (1 μmol/L) in the absence and presence of increasing concentrations of TBP (0–8: 0–120 μg/L with 15 μg/L intervals) after addition of HPCD (0.5 mmol/L) at 296, 303, 310 and 318 K, respectively. (i) Stern-Volmer plots for the TCP-HSA interaction in the presence of HPCD at 296, 303, 310 and 318 K, respectively. (j) Van't Hoff plot for the TCP-HSA interaction in the presence of HPCD. (k) Stern-Volmer plots for the TBP-HSA interaction in the presence of HPCD at 296, 303, 310 and 318 K, respectively. (l) Van't Hoff plot for the TBP-HSA interaction in the presence of HPCD.

without the presence of TCP/TBP, respectively. k_q is the quenching rate constant of HSA; as shown in Fig. S2, τ_0 is the average fluorescence lifetime of the macromolecule in the absence of ligands and the measured value is 5.639 ns (Table S1); K_{sv} is the Stern-Volmer quenching constant; [Q] is the concentration of TCP/TBP. As shown in Fig. 1i and Fig. 1k, the Stern-Volmer plots of fluorescence intensity for HSA quenched by TCP/TBP at temperatures of 296, 303, 310 and 318 K showed linear trends, and the slopes for each temperature decreased obviously with increment of temperature. Accordingly, the calculated values for k_q and K_{sv} at temperatures of 296, 303, 310 and 318 K are listed in Table 1, and the results showed that values for k_q and K_{sv} decreased with rising temperature, implying that the TCP/TBP-HSA interactions were dominated by static quenching mechanism. Besides, the values of quenching constant k_q for TCP and TBP were in the range of 0.710×10^{14}–4.060×10^{14} and 1.709×10^{14}–5.052×10^{14} L mol^{-1} s^{-1}, respectively, which are all higher than the maximum scatter collision quenching constant (2.0×10^{10} L mol^{-1} s^{-1}) reported for dynamic quenching (Rabbani, Baig, Lee, Cho, Ma, & Choi, 2017). Besides, the fluorescence lifetime measurements for HSA showed that lifetime (τ_0) of HSA only changed in less than 0.3 ns (Table S1) after addition of TCP/

Table 1
Binding and thermodynamic parameters for the interactions of HSA with TCP/TBP in the absence and presence of HPCD at different temperatures.

Ligand	T (K)	K_{SV} ($\times 10^6$ L mol^{-1})	R^2	k_q ($\times 10^{14}$ L mol^{-1} s^{-1})	K_a ($\times 10^7$ L mol^{-1})	ΔH^0 (kJ mol^{-1})	ΔS^0 (J mol^{-1} K^{-1})	$T\Delta S^0$ (kJ mol^{-1})	ΔG^0 (kJ mol^{-1})
TCP	296	2.290 ± 0.084	0.9906	4.060 ± 0.149	6.193	−142.34	−330.18	−97.73	−44.61
	303	1.568 ± 0.055	0.9916	2.780 ± 0.097	2.433			−100.05	−42.29
	310	0.883 ± 0.038	0.9869	1.565 ± 0.068	0.606			−102.36	−39.98
	318	0.400 ± 0.013	0.9922	0.710 ± 0.024	0.118			−105.00	−37.34
TBP	296	2.849 ± 0.146	0.9820	5.052 ± 0.259	9.091	−72.97	−95.36	−28.23	−44.74
	303	2.565 ± 0.107	0.9879	4.548 ± 0.190	3.226			−28.89	−44.08
	310	2.073 ± 0.067	0.9927	3.677 ± 0.119	2.016			−29.56	−43.41
	318	0.964 ± 0.036	0.9905	1.709 ± 0.063	1.099			−30.32	−42.65
TCP + HPCD	296	0.508 ± 0.010	0.9976	0.901 ± 0.017	0.110	−36.16	−7.27	−2.15	−34.01
	303	0.440 ± 0.011	0.9955	0.781 ± 0.020	0.064			−2.20	−33.96
	310	0.387 ± 0.004	0.9992	0.686 ± 0.007	0.049			−2.26	−33.91
	318	0.240 ± 0.005	0.9963	0.427 ± 0.013	0.039			−2.31	−33.86
TBP + HPCD	296	1.142 ± 0.056	0.9836	2.026 ± 0.099	0.213	−36.16	−58.82	−17.41	−35.32
	303	0.925 ± 0.073	0.9585	1.639 ± 0.129	0.082			−17.82	−34.91
	310	0.660 ± 0.024	0.9907	1.171 ± 0.043	0.055			−18.23	−34.50
	318	0.437 ± 0.014	0.9929	0.775 ± 0.025	0.047			−18.70	−34.03

TBP, confirming the static quenching mechanism. Thus, the static quenching mechanism existed in binding interactions between TCP/TBP and HSA was once again verified.

The binding constants for TCP/TBP-HSA interactions were calculated by using the most generally valid equation (Eq. (3)) as it considers both protein residual fluorescence and the concentration of bound or free ligand (van de Weert & Stella, 2011; Bakar, & Feroz, 2019):

$$\frac{F_0 - F}{F_0 - F_c} = \frac{[P]_t + [L]_t + \frac{1}{K_a} - \sqrt{\left([P]_t + [L]_t + \frac{1}{K_a}\right)^2 - 4[P]_t[L]_t}}{2[P]_t} \quad (3)$$

where F and F_0 represent the fluorescence in the presence and absence of the ligand, F_c is the residual fluorescence of fully saturated HSA, $[P]_t$ is the total protein concentration, $[L]_t$ is the ligand concentration, and K_a is the binding constant. Table 1 shows the calculated binding constants. It can be clearly seen from the table that the binding constants decreased with increasing of temperature owing to possible destabilization of the TCP/TBP-HSA complexes at higher temperatures, which further demonstrated the static quenching mechanism for the TCP/TBP-HSA interactions. The binding constants of both TCP-HSA and TBP-HSA at four different temperatures were in the range of 0.118×10^7–9.091×10^7 L mol^{-1}, which were much higher than 1×10^4 L mol^{-1}, suggesting that interactions for TCP-HSA and TBP-HSA are strong (Zhang, et al., 2019). The binding constants obtained from ITC were 0.937×10^5 L mol^{-1} for HSA-TCP interaction and 1.550×10^5 L mol^{-1} for HSA-TBP interaction (Table S2), which showed the same trend and can be comparable to binding constants gained from the fluorescence quenching data.

For the interactions of TCP-HSA and TBP-HSA in the presence of HPCD, the quenching constants k_q decreased significantly for both of the halophenol-HSA complexes compared to those observed without HPCD (Fig. 2 and Table 1). Besides, the calculated binding constants for TCP-HSA and TBP-HSA with the presence of HPCD decreased as well, e.g., the binding constant of TCP-HSA decreased from 6.193×10^7 to 0.110×10^7 L mol^{-1} at 296 K. These results indicated that either TCP or TBP molecule may be encapsulated in HPCD, and thus the presence of HPCD obstructed the interactions between DBPs and HSA macromolecule. As a result, the bioavailability and toxicity of TCP/TBP may be reduced by the introduction of HPCD.

3.3. Thermodynamic analysis

The interaction forces which account for protein–ligand interactions mainly include hydrogen bonding, electrostatic forces, van der Waals forces, and hydrophobic interactions (Xu et al., 2016). The binding mode and dominant binding forces could be determined by thermodynamic parameters, i.e., entropy change (ΔS^0), enthalpy change (ΔH^0) and change in Gibbs free energy (ΔG^0). The values of ΔH^0, ΔS^0, and ΔG^0 for the binding interactions between TCP/TBP and HSA were calculated using equation (4) (van't Hoff equation) and equation (5), and the results are listed in Table 1.

$$lnK_a = -\frac{\Delta H^0}{RT} + \frac{\Delta S^0}{R} \quad (4)$$

$$\Delta G^0 = \Delta H^0 - T\Delta S^0 \quad (5)$$

where K_a, R, and T represent the binding constant, the universal gas constant (which is equal to 8.3145 J mol^{-1} K^{-1}) and temperature. In this study, the negative ΔG^0 values (Table 1) indicated that the formation of TCP/TBP-HSA complexes was a spontaneous process (Rabbani, Lee, Ahmad, Baig, & Choi, 2018). A more negative ΔG^0 value could be found for TBP-HSA complex among TCP/TBP-HSA interactions for each temperature, suggesting a more stable binding mode for TBP-HSA

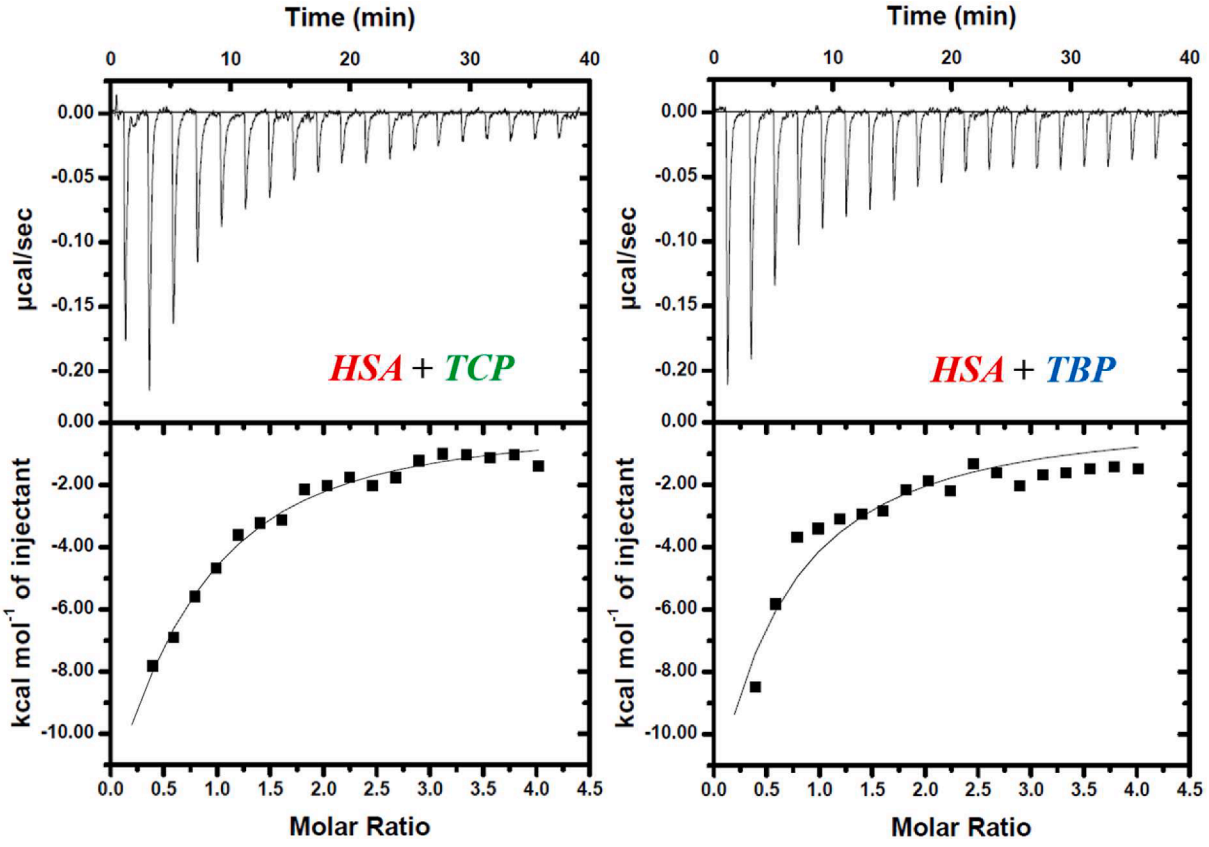

Fig. 3. HSA (10 μmol/L) calorimetric titration curves along various molar ratio ranges with titrant solutions of TCP (200 μmol/L) and TBP (200 μmol/L) at 37℃, respectively.

interaction compared to TCP-HSA interaction, which could also be confirmed by ITC data (Fig. 3) analysis as ΔG^0 value was –29.57 kJ mol^{-1} for TCP-HSA and –30.83 kJ mol^{-1} for TBP-HSA interaction at temperature of 310 K (Table S2), respectively. It could also be observed that ΔH^0 and ΔG^0 values for halophenol-HSA interactions were very close which obtained by fluorescence and ITC method. Notably, the result is in accordance with our previous studies that TBP showed relatively higher toxic potency than TCP based on *in vitro* (cell cytotoxicity) (Zhang, et al., 2020) and *in vivo* (developmental toxicity) (Yang & Zhang, 2013) bioassay data.

In addition, the dominant forces accounted for binding interaction could be well described by positive or negative values of ΔH^0 and ΔS^0, e.g. a positive ΔS^0 change indicates hydrophobic interactions, whereas a negative value of ΔS^0 suggests hydrogen binding and van der Waals forces interactions. In the present study, negative ΔH^0 and ΔS^0 can be found in all binding systems, which confirmed the existence of hydrogen bonding (Guo, Yuan, & Zeng, 2014). The ΔH^0 and ΔS^0 values obtained from ITC all showed negative values for both TCP-HSA and TBP-HSA interactions, which was believed to be more accurate for thermodynamic analysis as it directly measures the heat released or taken up during the interaction (Bouchemal, & Mazzaferro, 2012). Therefore, from the data given in Table 1, it could be suggested that hydrogen bonding and van der Waals forces played a major role in the binding of TCP and TBP with HSA (Guo, Yuan, & Zeng, 2014).

3.4. Esterase-like activity of HSA

The relative modulation of esterase-like activity for HSA in the presence of different molar ratios of HSA:TCP/TBP (1:0, 1:5, 1:10) were shown in Fig. S3 and the kinetic parameters were listed in Table S3. It can be observed that for either HSA-TCP or HSA-TBP interaction, K_m increased while v_{max} increased as well, indicating that binding of TCP/TBP to HSA didn't occupy its catalytic site in subdomain IIIA (Rabbani, Baig, Lee, Cho, Ma, & Choi, 2017), which agreed well with molecular docking analysis as described later. The progressive increase in the K_m value and decrease in catalytic efficiency (k_{cat}/K_m) indicated that binding of TCP/TBP to HSA triggered the conformational change, resulting in decrease of relative esterase activity. After addition of HPCD, this effect became less obvious, showing that HPCD could recover the conformation change by TCP/TBP. These results were in accordance with circular dichroism analysis as described later.

3.5. UV absorption and circular dichroism analysis

UV absorption spectroscopy is a simple and effective method which can be applied to confirm the formation of protein–ligand complex (Shen, et al., 2015). The UV absorption spectra of HSA in the presence of different concentrations of TCP/TBP were performed to investigate the conformational changes of HSA by addition of TCP/TBP and the results are shown in Fig. S4. The absorption peak at λ = 278 nm represents the absorption of the aromatic amino acids residues (Trp, Tyr, and phenylalanine) from HSA (Rabbani, Lee, Ahmad, Baig, & Choi, 2018). With increasing concentrations of TCP/TBP, the HSA absorbance maxima at λ = 278 nm increased, accompanying with an absorption peak at λ = 310 nm for TCP-HSA and 315 nm for TBP-HSA gradually appeared and increased, which can be attributed to the absorbance of TCP/TBP alone. These UV absorbance results further supported the previous conclusion that TCP/TBP could interact with HSA to from complexes, resulting in the alteration of HSA microenvironment, which became less hydrophobic (Vidhyapriya, Divya, Manimaran, & Sakthivel, 2019).

Circular dichroism spectroscopy can be applied as a powerful tool to measure the changes in the secondary structure of proteins causing by ligand binding interactions (Rabbani, Baig, Lee, Cho, Ma, & Choi, 2017). Interactions of TCP/TBP with HSA could perturb intermolecular or intramolecular forces, which as a result destroy the secondary structure of HSA to some extent (Fig. 4). The structure of HSA mainly constituted by α-helix, which can be characterized by two negative bands at approximately 208 and 222 nm (Rabbani, Baig, Lee, Cho, Ma, & Choi, 2017). With the addition of TCP/TBP, the intensities at 208 and 222 nm changed obviously, indicating the modification of secondary structure of HSA. The CDPro software was applied to further estimate the extent of HSA structure changes by calculation of fractions of α-helix, β-sheet, β-turn and random coil by using SELCON3 method (Sreerama & Woody, 2000). The results showed that when concentrations of TCP/TBP increased, partial loss of α-helical content can be found for the HSA structure, accompanying with increment of other fractions e.g. β-sheet, β-turn and random coil (Table S4). Thus, circular dichroism results evidently proved either TCP or TBP could cause the secondary structure changes of HSA through binding interactions, and TBP showed higher impact compared to TCP. It's also acknowledged that a protein's biological activity function is mainly associated with its the secondary structure, and a partial loss of α-helix content for HSA could result in its physiological dysfunction to some extent (Liu, Huang, Jiang, & Tuo, 2021).

With the addition of HPCD, the circular dichroism intensities of TCP/TBP-HSA binding systems showed a decreasing trend (Fig. 4), implying that the alterations of the HSA secondary structure could successfully be recovered by HPCD. The calculated fractions of secondary structure of HSA also supported this phenomenon (Table S4). The content of α-helical increased from 46.4% to 48.0% for TCP-HSA system and from 44.9% to 47.5% for TBP-HSA system, which is almost identical with the α-helical content of HSA alone (47.8%). The fluorescence sequential

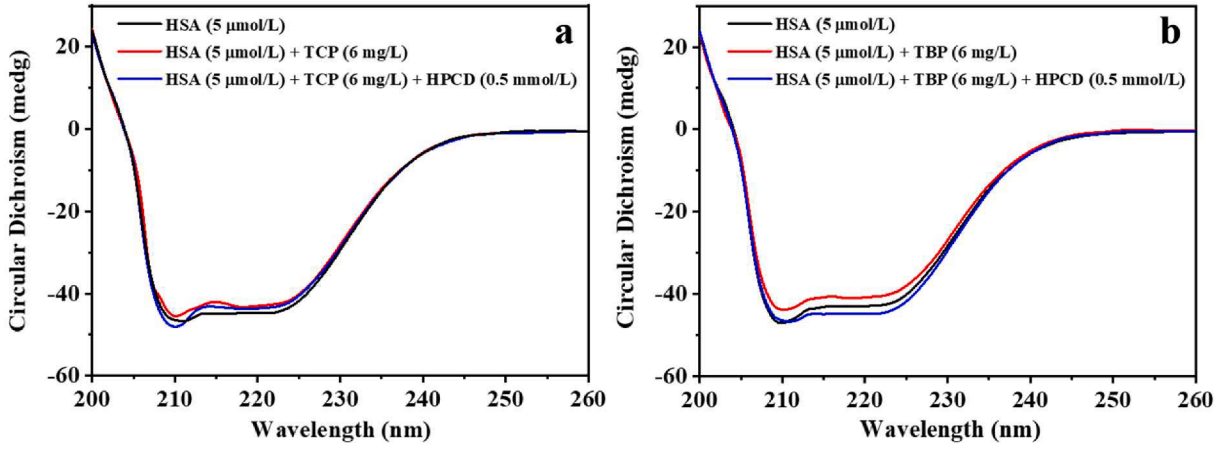

Fig. 4. (a) Circular dichroism spectra of HSA (5 μmol/L) in the absence and presence of TCP/HPCD. (b) Circular dichroism spectra of HSA (5 μmol/L) in the absence and presence of TBP/HPCD.

addition test could alternatively confirm this phenomenon. As displayed in Fig. S5, the fluorescence signal of HSA (1 μmol/L) firstly decreased to a certain level from around 26,000 (only HSA) to approximately 19,000 and 18,000 after addition of TCP and TBP (120 μg/L), respectively. After the addition of HPCD (0.5 mmol/L), the fluorescence recovered to around 21,000 and 20,000 for HSA-TCP and HSA-TBP binding systems, respectively.

3.6. Molecular docking analysis

Molecular docking analysis was carried out to further explore the binding mechanism in terms of binding energy calculation and binding sites prediction, as well as to explain the observed experimental results. The results of different binding modes by molecular docking are shown in Fig. 5 and Table S5. The overall 3D images illustrate that either TCP or TBP is able to transport into the central area of subdomain IB in HSA (Fig. 5a–d), which is far away from subdomain IIA that included residue Trp 214 (Ahmad et al., 2011). Hydrogen bonds can be found for both of TCP-HSA (LEU135) and TBP-HSA (TYR161) interactions (Fig. 5b and Fig. 5d). This phenomenon supported the above experimental results from the thermodynamic analysis that hydrogen bonding played major roles in complex formation between TCP/TBP and HSA.

The calculated binding affinity between TCP and HSA (–5.07 kcal mol^{-1}) is less negative than that between TBP and HSA (–5.83 kJ mol^{-1}) (Table S5), which follows the order of binding constants obtained from fluorescence spectroscopy, confirming that stronger interactions were found for TBP-HSA compared to TCP-HSA.

With the addition of HPCD, it is interesting to find that binding sites of TCP/TBP with HSA changed from subdomain IB to subdomain IIA accompanying by HPCD including them inside its cavity. Numerous studies have proved that CDs could act as a molecular cage which extract drugs that bound with serum albumin into its cavity through inclusion interactions (Naik, Pawar, & Tandel, 2018; Rahman, Afrin, & Tabish, 2018). Since HPCD could include hydrophobic compounds such as TCP/TBP into its cavity (Fig. 5e, f), the decrease of binding constants (Table 1), the recovery of fluorescence intensity (Fig. S5) and secondary structure change of HSA (Table S4) by HPCD could all be explained by this phenomenon. In the presence of HPCD, the binding energy for TCP-HSA interactions decreased from –5.07 to –6.10 kcal mol^{-1}. The triple-component binding system was more stable than the binary binding system. The inclusion of TCP into HPCD's cavity could lower down the binding interactions over TCP-HSA, and as a result lower down DBP availability towards HSA. The same trend could also be found for TBP-HSA interactions with binding energy decreased from –5.83 to –6.32 kcal mol^{-1}, and TBP-HPCD-HSA triple-component binding system was also more stable than the corresponding binary binding system. Five hydrogen bonds were found to be formed between HPCD and residues (GLN 104, HIS 247) of HSA, which reasonably made the binding more

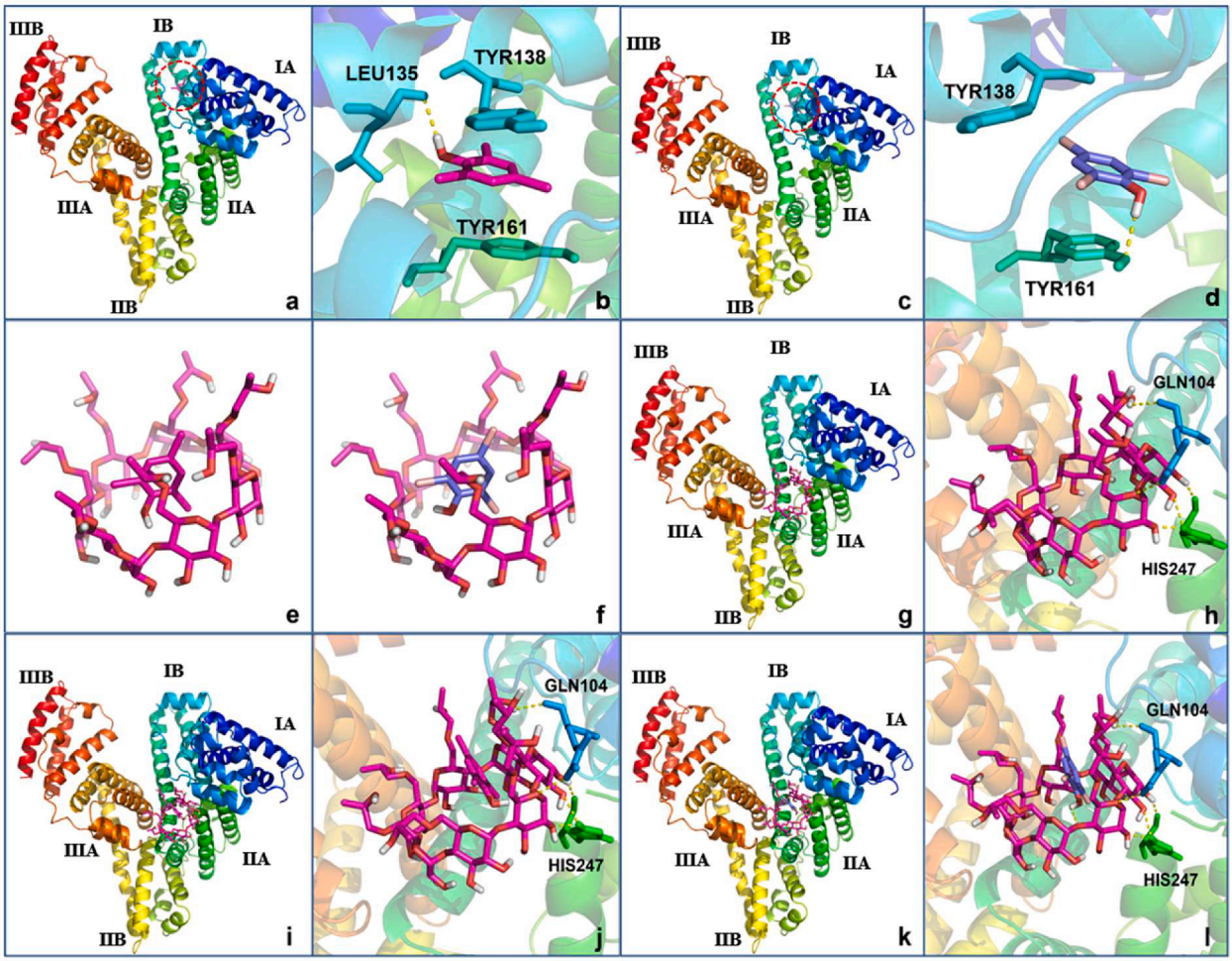

Fig. 5. (a, b) The lowest docking energy conformation of TCP-HSA and (c, d) TBP-HSA complex (the yellow dashed-line indicated hydrogen bonding). (e, f) The lowest docking energy conformation of TCP-HPCD and TBP-HPCD complexes. (g, h) The lowest docking energy conformation of HPCD-HSA complex (the yellow dashed-line indicated hydrogen bonding). (i, j) The lowest docking energy conformation of TCP-HSA complex in the presence of HPCD (the yellow dashed-line indicated hydrogen bonding). (k, l) The lowest docking energy conformation of TBP-HSA complex in the presence of HPCD (the yellow dashed-line indicated hydrogen bonding). (For interpretation of the references to colour in this figure legend, the reader is referred to the web version of this article.)

stable in the triple-component systems than the binary binding systems. In addition, the hydroxyl group from TCP/TBP could also form hydrogen bond with HPCD when being included. These docking results could clearly explain the fluorescence quenching results that the binding constants of either TCP-HSA or TBP-HSA decreased significantly after addition of HPCD. Thus, HPCD could lower down the degree of interactions between halophenols and HSA through including them into its hydrophobic cavity, accompanying with hydrogen bonds formed between its hydrophilic rim and residues of HSA, which further stabilized the interactions. Therefore, the bioavailability and toxicity of TCP/TBP tended to be decreased by the presence of HPCD. A previous study also reported that complexation of HPCD with butachlor can significantly reduce the toxicity of butachlor to fishes; with the presence of HPCD, the 96 h median lethal concentration value increased from 0.65 mg/L to 2.30 mg/L (Geng, Xie, Wang, Cai, Ma, & Ni, 2018).

Molecular docking analysis agreed well with the experimental results by using *in vitro* method, and the *in silico* method further revealed that the presence of HPCD could include either TCP or TBP into its cavity and changed their original binding sites from subdomain IB to IIA; moreover, compared to halophenol-HSA complexes, a more stable binding mode was found for HPCD-TCP-HSA and HPCD-TBP-HSA triple binding systems. Considering that HPCD is non-toxic and has been extensively used in the food industry mainly as food additives, it showed some potential promising application to decrease the toxicity of DBPs over human body when ingesting drinking water. The results of the present study would provide valuable suggestions for possible toxicity reduction of DBPs by using HPCD.

4. Conclusion

In summary, binding behaviors of two halogenated aromatic DBPs (TCP and TBP) with HSA were investigated by using *in vitro* (fluorescence quenching, UV absorbance, circular dichroism) and *in silico* (molecular docking) method. The experimental results indicated that TCP/TBP could bind with HSA to form halophenol-HSA complex, and TBP with a higher toxic potency also showed a higher binding affinity towards HSA. The binding interactions between TCP/TBP and HSA could occur spontaneously, and hydrogen bonding and van der Waals forces were found to be dominant forces that accounted for the stabilization of the complex. The binding of TCP/TBP to HSA changed the secondary structure of HSA as analyzed by UV absorption and circular dichroism spectroscopy. Notably, with the involvement of HPCD, binding constants of TCP-HSA and TBP-HSA complexes decreased obviously, and the initial change of the HSA secondary structure can be recovered to some extent. The molecular docking analysis results agreed well with the experimental results, and the modeling study further revealed that the presence of HPCD could encapsulated TCP/TBP into its cavity and changed their original binding sites from subdomain IB to IIA; moreover, compared to halophenol-HSA complexes, a more stable binding mode was found for HPCD-TCP-HSA and HPCD-TBP-HSA triple binding systems. Considering that HPCD is non-toxic, it showed some potential promising application to decrease the bioavailability and toxicity of DBPs over human body when ingesting drinking water. These findings facilitated better understanding of effects of CDs over HSA-ligand binding system.

CRediT authorship contribution statement

Zhenxuan Zhang: Conceptualization, Methodology, Formal analysis, Software, Writing – original draft. **Qingyao Zhu:** Methodology, Formal analysis, Investigation. **Wenjie Liang:** Methodology, Formal analysis, Investigation. **Zekun Han:** Formal analysis, Investigation. **Cui Huang:** Investigation. **An Liu:** Conceptualization. **Yujuan Lu:** Resources. **Jiang Ma:** Conceptualization. **Mengting Yang:** Conceptualization, Methodology, Writing – review & editing, Supervision, Funding acquisition.

Declaration of Competing Interest

The authors declare that they have no known competing financial interests or personal relationships that could have appeared to influence the work reported in this paper.

Acknowledgments

This work is supported by the National Natural Science Foundation of China (Grant Nos. 51978405, 51508335 and 52170100), Natural Science Foundation of Guangdong Province (Grant 2016A030310061), Shenzhen Basic Research Project (Grants JCYJ20170818091859147 and JCYJ20150525092940987), and Guangdong Basic and Applied Basic Research Foundation (Grant 2020B1515120092). We would like to thank the anonymous reviewer for his/her comments and suggestions that have improved the initial manuscript. We would also like to express our thanks to Dr. Su Qin from Core Research Facilites of Southern University of Science and Technology for his help in ITC data analysis.

Appendix A. Supplementary data

Supplementary data to this article can be found online at https://doi.org/10.1016/j.foodchem.2022.132349.

References

Ahmad, E., Rabbani, G., Zaidi, N., Singh, S., Rehan, M., Khan, M. M., … Langowski, J. (2011). Stereo-Selectivity of Human Serum Albumin to Enantiomeric and Isoelectronic Pollutants Dissected by Spectroscopy Calorimetry and Bioinformatics. *PloS one, 6*(11), e26186.

Bakar, K. A., & Feroz, S. R. (2019). A critical view on the analysis of fluorescence quenching data for determining ligand–protein binding affinity. *Spectrochimica Acta Part A: Molecular and Biomolecular Spectroscopy, 223*, Article 117337.

Bouchemal, K., & Mazzaferro, S. (2012). How to conduct and interpret ITC experiments accurately for cyclodextrin–guest interactions. *Drug Discovery Today, 17*(11-12), 623–629.

Chu, W., Li, D., Gao, N., Templeton, M. R., Tan, C., & Gao, Y. (2015). The control of emerging haloacetamide DBP precursors with UV/persulfate treatment. *Water Research, 72*, 340–348.

Crini, G. (2014). Review: A History of Cyclodextrins. *Chemical Reviews, 114*(21), 10940–10975.

Davis, M. E., & Brewster, M. E. (2004). Cyclodextrin-based pharmaceutics: Past, present and future. *Nature Reviews Drug Discovery, 3*(12), 1023–1035.

Eftink, M. R., & Ghiron, C. A. (1981). Fluorescence quenching studies with proteins. *Analytical Biochemistry, 114*(2), 199–227.

Geng, Q., Xie, J., Wang, X., Cai, M., Ma, H., & Ni, H. (2018). Preparation and Characterization of Butachlor/(2-Hydroxypropyl)-β-cyclodextrin Inclusion Complex: Improve Soil Mobility and Herbicidal Activity and Decrease Fish Toxicity. *Journal of Agricultural and Food Chemistry, 66*(46), 12198–12205.

Grellier, J., Rushton, L., Briggs, D. J., & Nieuwenhuijsen, M. J. (2015). Assessing the human health impacts of exposure to disinfection by-products — A critical review of concepts and methods. *Environment International, 78*, 61–81.

Guo, Q., Yuan, J., & Zeng, J. (2014). Binding of dihydromyricetin and its metal ion complexes with bovine serum albumin. *Biotechnology & Biotechnological Equipment, 28*(2), 333–341.

Li, Z., Wang, J., Chen, X., Hu, S., Gong, T., & Xian, Q. (2019). A novel molecularly imprinted polymer-solid phase extraction method coupled with high performance liquid chromatography tandem mass spectrometry for the determination of nitrosamines in water and beverage samples. *Food Chemistry, 292*, 267–274.

Liu, J., Zhang, X., Li, Y.u., Li, W., Hang, C., & Sharma, V. K. (2019). Phototransformation of halophenolic disinfection byproducts in receiving seawater: Kinetics, products, and toxicity. *Water Research, 150*, 68–76.

Liu, Z., Huang, X., Jiang, Z., & Tuo, X. (2021). Investigation of the binding properties between levamlodipine and HSA based on MCR-ALS and computer modeling. *Spectrochimica Acta Part A: Molecular and Biomolecular Spectroscopy, 245*, Article 118929.

Morris, G. M., Goodsell, D. S., Halliday, R. S., Huey, R., Hart, W. E., Belew, R. K., & Olson, A. J. (1998). Automated docking using a Lamarckian genetic algorithm and an empirical binding free energy function. *Journal of Computational Chemistry, 19*(14), 1639–1662.

Morris, G. M., Huey, R., Lindstrom, W., Sanner, M. F., Belew, R. K., Goodsell, D. S., & Olson, A. J. (2009). AutoDock4 and AutoDockTools4: Automated docking with selective receptor flexibility. *Journal of Computational Chemistry, 30*(16), 2785–2791.

Naik, R. S., Pawar, S. K., Tandel, R. D., & J, S. (2018). Insights into the mechanism of interaction of a thrombin inhibitor, dabigatran etexilate with human serum albumin and influence of β-cyclodextrin on binding: Spectroscopic and computational approach. *Journal of Molecular Liquids*, 251, 119–127.

Frisch, M. J., Trucks, G. W., Schlegel, H. B., Scuseria, G. E., Robb, M. A., Cheeseman, J. R., et al. (2009). *Gaussian 09*, Revision A.01. Gaussian, Inc., Wallingford CT.

Petitpas, I., Bhattacharya, A. A., Twine, S., East, M., & Curry, S. (2001). Crystal structure analysis of warfarin binding to human serum albumin: ANATOMY OF DRUG SITE I. *Journal of Biological Chemistry, 276*(25), 22804−22809.

Rabbani, G., Khan, M. J., Ahmad, A., Maskat, M. Y., & Khan, R. H. (2014). Effect of copper oxide nanoparticles on the conformation and activity of β-galactosidase. *Colloids and Surfaces B: Biointerfaces, 123*, 96–105.

Rabbani, G., Ahmad, E., Khan, M. V., Ashraf, M. T., Bhat, R., & Khan, R. H. (2015). Impact of structural stability of cold adapted Candida antarctica lipase B (CaLB): In relation to pH, chemical and thermal denaturation. *RSC Advances, 5*(26), 20115–20131.

Rabbani, G., Baig, M. H., Lee, E. J., Cho, W.-K., Ma, J. Y., & Choi, I. (2017). Biophysical study on the interaction between eperisone hydrochloride and human serum albumin using spectroscopic, calorimetric, and molecular docking analyses. *Molecular Pharmaceutics, 14*(5), 1656–1665.

Rabbani, G., Baig, M. H., Jan, A. T., Ju Lee, E., Khan, M. V., Zaman, M., … Choi, I. (2017). Binding of erucic acid with human serum albumin using a spectroscopic and molecular docking study. *International Journal of Biological Macromolecules, 105*, 1572–1580.

Rabbani, G., Lee, E. J., Ahmad, K., Baig, M. H., & Choi, I. (2018). Binding of tolperisone hydrochloride with human serum albumin: Effects on the conformation, thermodynamics, and activity of HSA. *Molecular Pharmaceutics, 15*(4), 1445–1456.

Rabbani, G., & Ahn, S. N. (2019). Structure, enzymatic activities, glycation and therapeutic potential of human serum albumin: A natural cargo. *International Journal of Biological Macromolecules, 123*, 979–990.

Rahman, Y., Afrin, S., & Tabish, M. (2018). Interaction of pirenzepine with bovine serum albumin and effect of β-cyclodextrin on binding: A biophysical and molecular docking approach. *Archives of Biochemistry and Biophysics, 652*, 27–37.

Richardson, S. (2003). Disinfection by-products and other emerging contaminants in drinking water. *TrAC Trends in Analytical Chemistry, 22*(10), 666–684.

Shen, L., Xu, H., Huang, F., Li, Y., Xiao, H., Yang, Z., … Li, Y. (2015). Investigation on interaction between Ligupurpuroside A and pepsin by spectroscopic and docking methods. *Spectrochimica Acta Part A: Molecular and Biomolecular Spectroscopy, 135*, 256–263.

Sreerama, N., & Woody, R. W. (2000). Estimation of protein secondary structure from circular dichroism spectra: Comparison of CONTIN, SELCON, and CDSSTR Methods with an Expanded Reference Set. *Analytical Biochemistry, 287*(2), 252–260.

Sun, Q., Yang, H., Tang, P., Liu, J., Wang, W., & Li, H. (2018). Interactions of cinnamaldehyde and its metabolite cinnamic acid with human serum albumin and interference of other food additives. *Food Chemistry, 243*, 74–81.

van de Weert, M., & Stella, L. (2011). Fluorescence quenching and ligand binding: A critical discussion of a popular methodology. *Journal of Molecular Structure, 998*(1-3), 144–150.

Vester-Christensen, M. B., Hachem, M. A., Svensson, B., & Henriksen, A. (2010). Crystal structure of an essential enzyme in seed starch degradation: Barley limit dextrinase in complex with cyclodextrins. *Journal of Molecular Biology, 403*(5), 739–750.

Vidhyapriya, P., Divya, D., Manimaran, B., & Sakthivel, N. (2019). Molecular interaction of manganese based carbon monoxide releasing molecule (MnCORM) with human serum albumin (HSA). *Bioorganic Chemistry, 92*, 103078.

Xu, Z.-Q., Yang, Q-Q., Lan, J.-Y., Zhang, J.-Q., Peng, W., Jin, J.-C., … Liu, Y. (2016). Interactions between carbon nanodots with human serum albumin and γ-globulins: The effects on the transportation function. *Journal of Hazardous Materials, 301*, 242–249.

Yang, M., & Zhang, X. (2013). Comparative developmental toxicity of new aromatic halogenated DBPs in a chlorinated saline sewage effluent to the marine polychaete *platynereis dumerilii*. *Environmental Science & Technology, 47*(19), 10868–10876.

Ye, Y., Wu, T., Jiang, X., Cao, J., Ling, X., Mei, Q., … Shen, Y. (2020). Portable Smartphone-Based QDs for the Visual Onsite Monitoring of Fluoroquinolone Antibiotics in Actual Food and Environmental Samples. *ACS Applied Materials & Interfaces, 12*(12), 14552–14562.

Zhang, C.-L., Liu, J.-C., Yang, W.-B., Chen, D.-L., & Jiao, Z.-G. (2017). Experimental and molecular docking investigations on the inclusion mechanism of the complex of phloridzin and hydroxypropyl-β-cyclodextrin. *Food Chemistry, 215*, 124–128.

Zhang, C., Guan, J., Zhang, J., Yang, J., Wang, X., & Peng, X. (2021). Protective effects of three structurally similar polyphenolic compounds against oxidative damage and their binding properties to human serum albumin. *Food Chemistry, 349*, 129118.

Zhang, Y., Wu, S., Qin, Y., Liu, J., Liu, J., Wang, Q., … Zhang, H. (2018). Interaction of phenolic acids and their derivatives with human serum albumin: Structure–affinity relationships and effects on antioxidant activity. *Food Chemistry, 240*, 1072–1080.

Zhang, Z., Yang, M., Yi, J., Zhu, Q., Huang, C., Chen, Y., … Zhao, X. (2019). Comprehensive insights into the interactions of two emerging bromophenolic DBPs with human serum albumin by multispectroscopy and molecular docking. *ACS Omega, 4*(1), 563–572.

Zhang, Z., Zhu, Q., Huang, C., Yang, M., Li, J., Chen, Y., … Zhao, X. (2020). Comparative cytotoxicity of halogenated aromatic DBPs and implications of the corresponding developed QSAR model to toxicity mechanisms of those DBPs: Binding interactions between aromatic DBPs and catalase play an important role. *Water Research, 170*, 115283.